Biol. Cybernetics 34, 137–150 (1979)

Biological Cybernetics

A Mathematical Theory of Visual Hallucination Patterns*

G. B. Ermentrout** and J. D. Cowan***

Department of Biophysics and Theoretical Biology, The University of Chicago, Chicago, Illinois, USA

Abstract. Neuronal activity in a two-dimensional net is analyzed in the neighborhood of an instability. Bifurcation theory and group theory are used to demonstrate the existence of a variety of doubly-periodic patterns, hexagons, rolls, etc., as solutions to the field equations for the net activity. It is suggested that these simple geometric patterns are the cortical concomitants of the "form constants" seen during visual hallucinosis.

§ 1. Introduction

Hallucinations have fascinated mankind for centuries, but only recently have scientists begun to investigate their forms and mechanisms. They occur ubiquitously in a variety of different situations; auras preceding petit man epilepsy (Horwitz et al., 1967), hypnagogic hallucinations (Dybowski, 1939), fortification patterns of migraine headaches (Richards, 1971), drug-induced hallucinations (Brawley and Duffield, 1972; Siegel, 1978) as well as many other conditions (Klüver, 1967; Lance, 1976). We shall be primarily concerned with the phenomena accompanying the early stages of drug-induced visual hallucinations. These stages are characterized by the appearance of many simple geometric structures which are apparently context-free and independent of previous experiences (Siegel, 1977). It is these simple forms which we wish to analyze.

Until Klüver (1967) began a series of extensive experiments on mescaline-induced hallucinations, no attempt had ever been made to classify the forms of simple visual hallucinations. He observed that regardless of the cause of the sensory irregularity, almost all simple hallucinations could be classified into one of the following four categories of "form constants" (Klüver, 1967):

a) grating, lattice, fretwork, filigree, honeycomb, or chessboard;

b) cobweb;

c) funnel, tunnel, cone, or vessel;

d) spiral.

"The tendency toward geometrization as expressed in these form constants is also apparent in the following two ways: a) the forms are frequently repeated, combined, or elaborated into ornamental designs and mosaics of various kinds; b) the elements constituting the forms have boundaries consisting of geometric forms" (Klüver, 1967, p. 66).

The patterns are of two main types; small repetitive "mosaics" [forms a) and b)] and more "global" patterns [forms c) and d)]. In Fig. 1 we show examples of the various patterns observed by hallucinating subjects. In Fig. 1a we see lattice or fretwork hallucinations characterized by small repeating geometric tesselations of visual space. Figure 1b depicts a typical cobweb or spiderweb illusion; in some sense it is similar to Fig. 1a except that it is distorted. Figure 1d shows two types of "tunnel" or "funnel" hallucinations, both taken from Siegel (1977). Finally a typical spiral form constant is pictured in Fig. 1c.

The next obvious question, now that the simple patterns have been classified, is "where do they originate?". Some experimentalists believe visual hallucinations occur as a result of light hitting various structures in the eyeball: network and lattice forms could be due to the web of intraoccular blood vessels, etc. Experiments performed in total darkness in which subjects consistently hallucinate would seem to disprove this theory (Siegel, 1977). Krill (1963) found that 1 μg/kg doses of LSD produced visual hallucinations in 13 of 16 blind subjects who normally had spontaneous visual experiences (SVE). Since some of the

* To Heinrich Klüver in memoriam

** *Current address:* Mathematical Research Branch, NIAMDD, NIH, Bethesda, MD 20014, USA

*** Supported in part by NIH TG 2037

0340-1200/79/0034/0137/$02.80

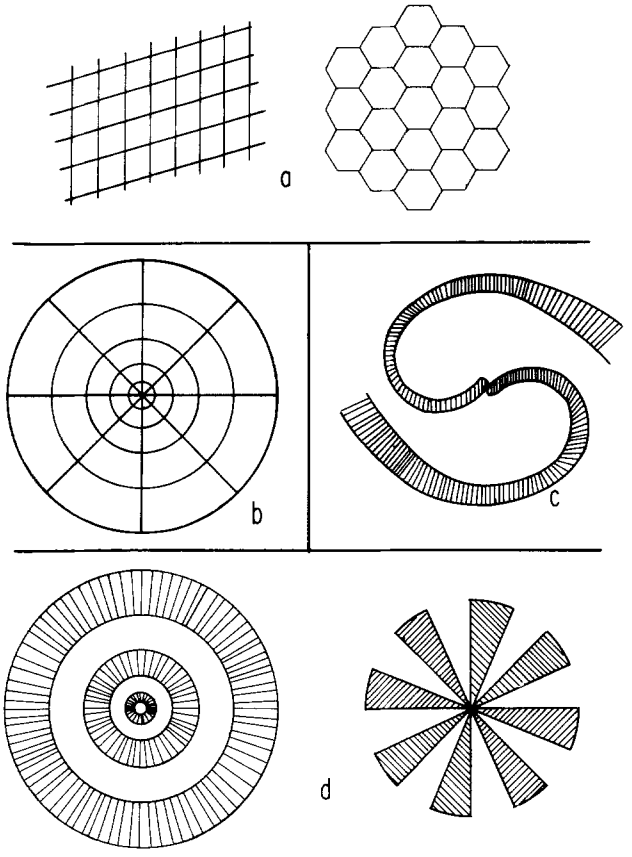

Fig. 1. **a** Typical lattice form constants. **b** Cobweb form constant. **c** Spiral form constant. **d** Tunnel and funnel constants

subjects were completely enucleated, any visual experience must have arisen from higher processes. Penfield and Perot (1963) evoked auditory, somatosensory, and visual hallucinations by stimulating the temporal cortex of human subjects. Similarly Horowitz and others found that multiple electrodes in subcortical regions of the temporal lobe elicited visual experiences (Horwitz et al., 1967). These experiments, coupled with the complex imagery which occurs in the later stages of hallucinosis, suggest that the origin of the simple pattern is cortical, not peripheral.

Assuming that hallucinations are cortical in origin, we discuss the possible causes of the irregularities generating the patterns. We assert that an increase in cortical excitability is necessary for the onset of hallucinosis. Indeed the EEG is similar to the pattern associated with arousal; intermittent hypersynchrony superimposed over the usual low voltage fast activity pattern (Winters and Wallach, 1970). After injection of LSD, similar EEG patterns are seen in cats concomitant with bizarre postures and inappropriate behaviors (Adey et al., 1962). A large amount of evidence has accumulated indicating that this cortical excitability is mediated through disinhibition in the brainstem (Demetrescu, 1967). LSD has been found to exert an inhibitory effect on the neurons of the Raphe nucleus (Aghajanian et al., 1970) which project inhibitory serotonergic fibers to the cortex (Fuxe, 1965). Thus it is a tempting proposal to assert that this disinhibition is responsible for the enhanced cortical excitability. Unfortunately, the story does not end here. Some experiments (Pieri et al., 1978) have demonstrated that disinhibition by blocking the Raphe nuclei is not sufficient to induce hallucinations in humans. Consequently there must be other influences modulating cortical excitability. As to the nature of these influences, very little is known, so we shall assume their existence, leaving verification or refutation for later experiments.

The above experimental evidence leads us to our main contention: simple formed hallucinations arise from an instability of the resting state leading to concomitant spatial patterns of activity in the cortex. This instability arises from a combination of enhanced excitatory modulation and decreased inhibition (disinhibition). We shall demonstrate that such spatial patterns are a property of neural nets with strong lateral interactions acting to provide a dominant negative feedback. In the following sections we formalize these postulates into a simple mathematical model and than use bifurcation theory to demonstrate the existence of the relevant spatial patterns.

§ 2. Form Constants and their "Appearance" at the Cortical Level

A variety of experimental observations, anatomical, physiological, and psychophysical, have established in primates, and presumably also in humans, that there is a *conformal* projection of the visual field, onto the visual cortex (Cowan, 1978). Since the retina has approximate radial symmetry, and the cortex translational symmetry (Fischer, 1973), it follows that there must be a nonlinear coordinate transformation from retinal polar coordinates (ϱ, θ) to cortical rectangular coordinates (x, y). This transformation has been shown to take the detailed form (Cowan, 1978)

$$x = \sqrt{\frac{4k}{\pi\varepsilon}} \cdot \ln[(\sqrt{\varepsilon}\varrho + (w_0^2 + \varepsilon\varrho^2)^{1/2})/2w_0],$$

$$y = \sqrt{\frac{4k}{\pi\varepsilon}} \cdot \frac{\varrho\theta}{\sqrt{(w_0^2 + \varepsilon\varrho^2)}},$$

where ϱ denotes the radial distance (in degrees of visual angle) from the center of the visual field, the fovea, θ the corresponding angular coordinate; and the constants w_0, ε, and k, respectively, the mean diameter of foveal ganglion cells, the rate of increase of the mean diameter of such cells with ϱ, the number of receptive field centers within the center of a given ganglion cell.

It will be seen that close to the fovea, ϱ small,

$$x=\sqrt{\frac{4k}{\pi}}\varrho w_0^{-1}, \quad y=\sqrt{\frac{4k}{\pi}}\varrho\theta w_0^{-1}$$

i.e., polar coordinates in disguise, whereas sufficiently far away from the fovea, $\varrho>1°$,

$$x=\sqrt{\frac{4k}{\pi\varepsilon}}\cdot\ln\left[\frac{\sqrt{\varepsilon}}{w_0}\varrho\right], \quad y=\sqrt{\frac{4k}{\pi\varepsilon}}\cdot\theta.$$

This is the complex logarithm (Cowan, 1977; Schwartz, 1977). Thus, a point on the retina may be represented by $z=\frac{\sqrt{\varepsilon}}{w_0}\varrho e^{i\theta}$ and the corresponding point on the visual cortex by the complex logarithm

$$w=\sqrt{\frac{4k}{\pi\varepsilon}}\ln z$$
$$=\sqrt{\frac{4k}{\pi\varepsilon}}\ln\left[\frac{\sqrt{\varepsilon}}{w_0}\varrho\right]+i\sqrt{\frac{4k}{\pi\varepsilon}}\cdot\theta,$$

for sufficiently large ϱ. Schwartz (1977) has discussed such a map in terms of the retino-cortical magnification factor, a notion also discussed by Cowan (1977, 1978). Our purpose here is to show the effect of this map on the form constants "seen" during hallucinations and consequently classify the corresponding patterns of activity on the cortex. We note that one of the differences between cobwebs and lattice constants is that the latter occur at the periphery, while the former are nearer to the fovea. In fact, the figures in Siegel (1977) demonstrate a marked tendency of the patterns to curve toward the center of vision. This may be viewed as further evidence for the cortical origin of visual hallucinations. Except for distortions of shape, the local patterns (a) and (b) remain virtually unchanged under the retino-cortical map, as we except from the above discussion. In Figs. 2a and b we show the cortical patterns corresponding to the honeycomb and cobweb form constants.

In contrast to the local patterns above, the other form constants (tunnels, funnels, and spirals) cover the entire visual field with relatively large components. Consider, first, a typical tunnel pattern consisting of concentric circles of "activity". This transforms to a pattern of periodic lines constant along the y-axis (Fig. 2c). The "white-light" funnel pattern transforms to periodic lines constant along the x-axis (Fig. 2d). Finally, the spiral pattern transform to a series of periodic patterns constant along lines of some finite slope (see Fig. 2e). Both the tunnel (Fig. 2c) and funnel (Fig. 2d) are degenerate cases of the spiral; (Fig. 2c) consists of lines with infinite slope while (Fig. 2d) consists of lines with zero slope.

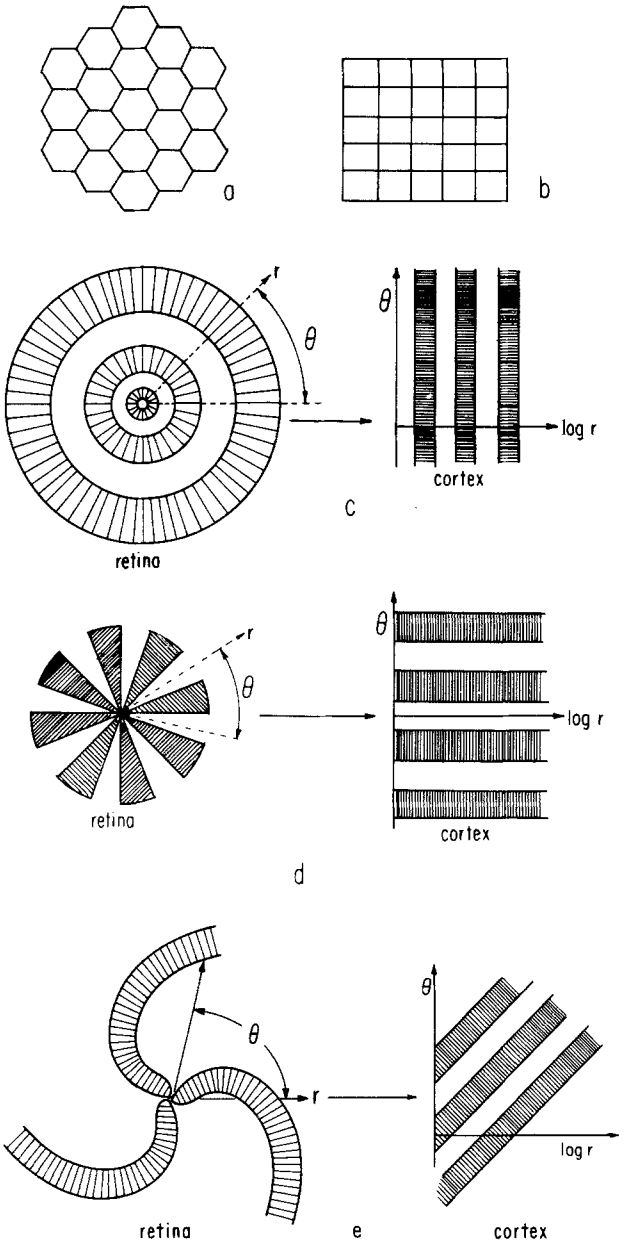

Fig. 2. a Pattern of a typical lattice at the cortical level. **b** Pattern of cobweb on the cortex. **c** Transformation of tunnel form constant via retino-cortical map to cortex. **d** Same, for funnel constant. **e** Same, for spiral constant

In conclusion, we can now classify the form constants of visual hallucinations in terms of cortical coordinates. They are of two main classes: (i) cellular patterns consisting of hexagons, squares, and rectangles, and (ii) "rolls", consisting of patterns constant along some direction vector. Both classes are within the class of doubly-periodic patterns in the plane; that is, if we denote the "amplitude" of activity recorded at a point (x, y) in cortical coordinates, we see that $A(x+\omega_1, y+\omega_2)=A(x, y)$ where (ω_1, ω_2) is some point in a lattice (see Part 5).

§ 3. Objectives and Model

Our objective is to demonstrate that a simple isotropically connected two-layer neural net admits stable doubly-periodic stationary states as solutions, when the rest state is unstable to certain perturbations. We assume the cortex consists of two types of neurons, excitatory and inhibitory, with the following properties:

1. With each neuron there is an associated membrane potential, V_j.

2. The output current, I_j, of the neuron is a nonlinear function of the potential, $I_j = S(V_j)$.

3. The influence of neuron j on neuron k depends on some absolute synaptic "weight" w multiplied by a probability depending only on the distance $|j-k|$: $\psi_{jk} = \alpha w(|j-k|) I_j$.

4. The response of the dendrite Φ_{jk}, is a function of the temporal properties of the stimulus and of the dendritic membrane:

$$\Phi_{jk} = \int_{-\infty}^{t} h(t-\tau)\psi_{jk}(\tau)d\tau .$$

Here $h(t)$ is a temporal response function incorporating delays, rise times, and decay rates. To simplify analysis, we assume $h(t) = \exp(-t/\mu)/\mu$, thus the dendrite is a simple R–C-network with $\mu = RC$, the time constant.

5. The total membrane potential V_k is the sum of the postsynaptic potentials.

Thus we obtain:

$$I_k(t) = S\left(\sum_j \Phi_{jk}\right) = S\left[\sum_j \int_{-\infty}^{t} h(t-\tau)\alpha w(|j-k|) I_j(\tau)d\tau\right]. \tag{3.1}$$

Let $E(x, y, t)$ and $I(x, y, t)$ denote the currents or firing rates of the excitatory and inhibitory neurons at a point (x, y) at time t. Then in the continuum limit of (3.1), we obtain:

$$\begin{aligned} E(x,y,t) = S_e\Bigg[& \int_{-\infty}^{t} d\tau h_e(t-\tau) \int_{-\infty}^{\infty} dx' \int_{-\infty}^{\infty} dy' \\ & \cdot \{\alpha_{ee} w_{ee}((x-x')^2+(y-y')^2) E(x',y',\tau) \\ & - \alpha_{ie} w_{ie}((x-x')^2+(y-y')^2) I(x',y',\tau)\}\Bigg], \end{aligned} \tag{3.2}$$

$$\begin{aligned} I(x,y,t) = S_i\Bigg[& \int_{-\infty}^{t} d\tau h_i(t-\tau) \int_{-\infty}^{\infty} dx' \int_{-\infty}^{\infty} dy' \\ & \cdot \{\alpha_{ei} w_{ei}((x-x')^2+(y-y')^2) E(x',y',\tau) \\ & - \alpha_{ii} w_{ii}((x-x')^2+(y-y')^2) I(x',y',\tau)\}\Bigg]. \end{aligned}$$

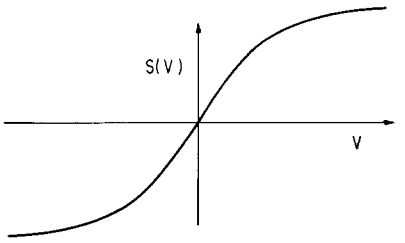

Fig. 3. Nonlinear threshold function for a neural net

Here α_{mn} denote the absolute synaptic strength between cells of type m and cells of type n, $w_{mn}((x-x')^2 + (y-y')^2)$ are the probability weights dependent only on $(x-x')^2+(y-y')^2$. S_e and S_i are the characteristic output functions of the excitatory and inhibitory cells. There is adequate physiological evidence (Schwindt, 1973) that these function satisfy:

(i) $S_m(v)$ is monotone nondecreasing;
(ii) $S_m(v)$ is bounded as $v \to \pm\infty$; (3.3)
(iii) $S_m(v)$ has a unique inflection point called the threshold (see Fig. 3).

Finally without loss in generality, we may assume $S_m(0) = 0$. It is clear from (3.2) that all solutions to the equation are bounded by the bounds of S_e and S_i. For notational convenience let $w^{**}z$ denote the double convolution:

$$\int_{-\infty}^{\infty} dx' \int_{-\infty}^{\infty} dy' w(x-x', y-y') z(x', y').$$

When $h_e(t) = h_i(t) = \exp(-t)$, then (3.2) takes the form:

$$\begin{aligned} \frac{\partial \hat{E}}{\partial t} &= -\hat{E} + S_e(\alpha_{ee} w_{ee}^{**} \hat{E} - \alpha_{ie} w_{ie}^{**} \hat{I}) \\ \frac{\partial \hat{I}}{\partial t} &= -I + S_i(\alpha_{ei} w_{ei}^{**} \hat{E} - \alpha_{ii} w_{ii}^{**} \hat{I}), \end{aligned} \tag{3.4}$$

where

$$\begin{pmatrix} \hat{E} \\ \hat{I} \end{pmatrix} = \int_{-\infty}^{t} \exp(-(t-\tau)) \begin{pmatrix} E(\tau) \\ I(\tau) \end{pmatrix} d\tau .$$

We shall drop the "^" notation, keeping in mind that the variables are now time course grained. The connection functions, $w_{mn}(x^2+y^2)$ are assumed to be of the form: $w_{mn}(x^2+y^2) = w((x^2+y^2)/\sigma_{mn}^2)/\sigma_{mn}^2$ where σ_{mn} are space constants determining the rate of decay of connectivity with radial distance, $r = \sqrt{x^2+y^2}$. w satisfies

(i) $w(r) \geqq 0$.

(ii) $\int_{-\infty}^{\infty} dx' \int_{-\infty}^{\infty} dy' w(x'^2+y'^2) = 1$. (3.5)

(iii) $\hat{w}(k^2+\ell^2) = \int_{-\infty}^{\infty} dx' \int_{-\infty}^{\infty} dy' w(x'^2+y'^2) e^{i\ell x'} e^{iky'}$

is decreasing as a function of $\omega^2 = k^2+\ell^2$.

Many functions satisfy (3.5), in particular the exponential and Gaussian functions:

$$w(x^2+y^2)=\exp(-\sqrt{(x^2+y^2)}/2\pi, \tag{3.6a}$$

$$w(x^2+y^2)=\exp(-(x^2+y^2))/\pi \tag{3.6b}$$

with corresponding transforms:

$$\hat{w}(\mathcal{k}^2+\ell^2)=1/(1+\ell^2+\mathcal{k}^2)^{3/2}, \tag{3.7a}$$

$$\hat{w}(\mathcal{k}^2+\ell^2)=\exp(-(\ell^2+\mathcal{k}^2)/4). \tag{3.7b}$$

Choosing connection functions which depend only on radial distance is equivalent to assuming cortical connectivity is isotropic. This is not an unreasonable approximation, as the cortex appears almost crystalline and homogeneous in the large. We remark, that if $w_{mn}(x^2+y^2)=w((x^2+y^2)/\sigma_{mn}^2)/\sigma_{mn}^2$, then $\hat{w}_{mn}(\mathcal{k}^2+\ell^2)=w((\mathcal{k}^2+\ell^2)\sigma_{mn}^2)$.

In all experimental observations, the form constants remained approximately stationary. Thus we seek time independent solutions to (3.4) which satisfy:

$$\begin{aligned}&[E-S_e(\alpha_{ee}w_{ee}^{**}E-\alpha_{ie}w_{ie}^{**}I)]\triangleq G_e(E,I)=0\\&[I-S_i(\alpha_{ei}w_{ei}^{**}E-\alpha_{ii}w_{ii}^{**}I)]\triangleq G_i(E,I)=0.\end{aligned} \tag{3.8}$$

§ 4. Stability and Degeneracy

An important property of (3.6) is that it is rotationally and translationally invariant. Let $\mathcal{O}(2)$ denote the group of 2×2 matrices, A, satisfying $AA^t=I$, where I is the 2×2 identity matrix. This is the group of rotations and reflections in the plane. Let $\mathcal{E}$ denote the group of rigid motions in the plane. Each element, $g\in\mathcal{E}$, may be written as $g=\{r,\mathbf{a}\}$ where $r\in\mathcal{O}(2)$ is a rotation-reflection and $\mathbf{a}\in\mathbb{R}^2$ is a translation. Suppose that S_e and S_i are both $\mathcal{C}^k$ functions. Let $\mathcal{I}$ denote the Banach space of continuously k-times differentiable functions from R^2 into R^2, with the norm:

$$|\mathbf{u}(x,y)|_k=\sum_{|j|=0}^{k}|\partial^j\mathbf{u}(x,y)|_0.$$

Here

$$|\mathbf{u}|_0=\sup_{x,y}|u_1(x,y)|+\sup_{x,y}|u_2(x,y)|$$

and if

$$j=(j_1,j_2),\quad |j|=j_1+j_2,$$

and

$$\partial^j=\frac{\partial^{|j|}}{\partial x^{j_1}\partial y^{j_2}}.$$

The operator $\mathbf{G}\equiv\begin{pmatrix}G_e\\G_i\end{pmatrix}$ maps $\mathcal{I}$ into itself. For each element $g\in\mathcal{E}$, let $g\mathbf{x}=r\mathbf{x}+\mathbf{a}$ for $\mathbf{x}=(x,y)\in R^2$. We define a linear operator on $\mathcal{I}$ as follows. Let $\mathbf{u}\in\mathcal{I}$, then

$$(T_g\mathbf{u})(x)=\mathbf{u}(g^{-1}\mathbf{x}). \tag{4.1}$$

Clearly $T_{g_1}T_{g_2}=T_{g_1g_2}$ where $g_1g_2=(r_1r_2, r_1\mathbf{a}_2+\mathbf{a}_1)$ and $T_\varepsilon=I$ where $\varepsilon=(1,0)$ is the identity in $\mathcal{E}$. Because of the isotropicity condition on the connection function $w_{mn}(x^2+y^2)$, the nonlinear operator, $\mathbf{G}(E,I)$ commutes with T_g for each $g\in\mathcal{E}$:

$$T_g\mathbf{G}=\mathbf{G}T_g.$$

The proof of this is in Appendix A. Thus the system (3.8) has a very important symmetry property and it is this symmetry which enables us to readily calculate the form constants.

The solution, $E=I=0$, referred to as the rest state, will be the physically observed state as long as it is stable to small perturbations. Because of our discussion in § 1, it will be assumed that there is some parameter, λ, modulating the excitability of the net, say $\alpha_{ee}=\alpha_{ee}\lambda$ and $\alpha_{ei}=\alpha_{ei}\lambda$. Thus as λ increases, the strength of the excitation increases and the system becomes more excited. We wish to show that with strong lateral interactions of "negative feedback" type, a continuous increase in λ beyond some critical value, λ_0, leads to instability of the rest state and concomitant stationary spatial patterns of activity. Let us examine the linearized stability of the rest state for (3.7):

$$\begin{bmatrix}\frac{\partial E}{\partial t}\\[2mm]\frac{\partial I}{\partial t}\end{bmatrix}=\begin{bmatrix}-E+S_e'(0)[\alpha_{ee}\lambda w_{ee}^{**}E-\alpha_{ie}w_{ie}^{**}I]\\-I+S_i'(0)[\alpha_{ei}\lambda w_{ei}^{**}E-\alpha_{ii}w_{ii}^{**}I]\end{bmatrix}=L(\lambda)\begin{bmatrix}E\\I\end{bmatrix}. \tag{4.2}$$

This has solutions:

$$\begin{pmatrix}E(x,y,t)\\I(x,y,t)\end{pmatrix}=\Phi(\lambda,k,\ell)\exp[\nu(\lambda,k,\ell)t+ikx+i\ell y], \tag{4.3}$$

where $\nu(\lambda,k,\ell)$ and $\Phi(\lambda,k,\ell)$ are the eigenvalues and corresponding eigenfunctions of the 2×2 matrix:

$$H(\lambda,k^2+\ell^2)\equiv\begin{bmatrix}-1+S_e'(0)\alpha_{ee}\lambda\hat{w}_{ee}(k^2+\ell^2) & -S_e'(0)\alpha_{ie}\hat{w}_{ie}(k^2+\ell^2)\\S_i'(0)\alpha_{ei}\lambda\hat{w}_{ei}(k^2+\ell^2) & -1-S_i'(0)\alpha_{ii}\hat{w}_{ii}(k^2+\ell^2)\end{bmatrix}. \tag{4.4}$$

Clearly $\hat{w}_{nm}(k^2+l^2)$ depends only on the amplitude of the wave vector, $\omega^2=k^2+\ell^2$, thus we can parameterize Φ and ν by ω^2 and λ alone, i.e., $\Phi=\Phi(\lambda,\omega^2)$ and $\nu=\nu(\lambda,\omega^2)$. Let $\nu'(\lambda,\omega^2)$ be the eigenvalue of $H(\lambda,\omega^2)$ with maximal real part (since H is 2×2, there are only two eigenvalues for each λ and ω^2). For a fixed value of λ, we say the rest state, $E=I=0$, is stable if and only if

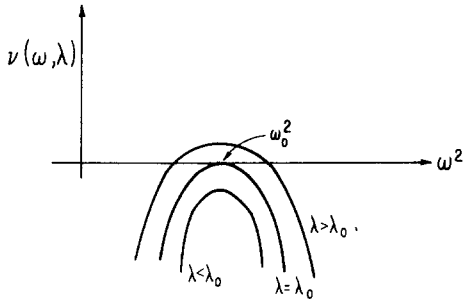

Fig. 4. Illustration of "dispersion" assumption (see text)

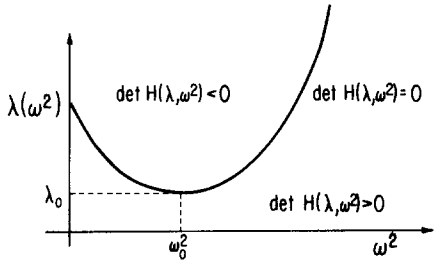

Fig. 5. Curve of critical values of λ for zero eigenvalue

$\mathrm{Re}\, \nu'(\lambda, \omega^2) \leqq 0$ for all ω. Otherwise the solutions (4.3) for the perturbations will grow exponentially in time. We assume that as λ increases there is some critical value, λ_0, at which $\mathrm{Re}\, \nu'$ vanishes for $\omega = \omega_0 \neq 0$ and remains negative for all other $\omega \neq \omega_0$. This motivates the following assumption:

(i) There is a $\lambda = \lambda_0$, say $\lambda_0 = 1$, and an $\omega_0^2 > 0$, such that for all $|\omega^2 - \omega_0^2| < \delta_1$, $|\lambda - \lambda_0| < \delta_2$, $H(\lambda, w^2)$ has a unique eigenvalue with maximal real part, $\nu'(\lambda, \omega^2)$ and it is real and simple.

(ii) Let $I_\lambda = \{\omega^2 | \nu'(\lambda, \omega^2) \geqq 0\}$. Then we assume (4.5)

$$I_\lambda = \begin{cases} \emptyset \text{ for } \lambda_0 - \delta_1 < \lambda < \lambda_0 \\ \omega_0^2 \text{ for } \lambda = \lambda_0, \omega_0^2 > 0 \\ \text{bounded interval of positive length for} \\ \lambda_0 < \lambda < \lambda_0 + \delta_1 . \end{cases}$$

We have illustrated this assumption in Fig. 4. An alternative viewpoint is to notice that $\nu'(\lambda, \omega_0^2) = 0$ if and only if $\det H(\lambda, \omega^2) = 0$. We thus obtain a relation between λ and ω^2. The ω_0^2 corresponding to minimal λ_0 is precisely the ω_0 of (4.5) (see Fig. 5). Essentially these assumptions embody the fact that as λ increases beyond λ_0, the rest state becomes unstable to perturbations of a wave number near ω_0^2. In order that the solutions which "branch" from the rest state as λ increases are not spatially constant, it is required that $\omega_0^2 \neq 0$. The following lemma shows that strong lateral interactions of negative feedback type are necessary for $\omega_0^2 \neq 0$.

Lemma 4.1. *A necessary condition for* $\omega_0^2 \neq 0$ *is*

$$\alpha_{ei}\alpha_{ie}[\sigma_{ei}^2 + \sigma_{ie}^2] > \alpha_{ee}\alpha_{ii}[\sigma_{ii}^2 + \sigma_{ee}^2] + \frac{\sigma_{ee}^2 \alpha_{ee}}{S_i'(0)} - \frac{\sigma_{ii}^2 \alpha_{ii}}{\lambda_0 S_e'(0)} . \tag{4.6}$$

This was proved in [8].

Finally, in order that Fig. 4 obtain, we require the eigenvalue $\nu'(\lambda, \omega^2)$ to actually increase as λ crosses λ_0, thus $\frac{\partial}{\partial \lambda} \nu'(\lambda, \omega_0^2)|_{\lambda = \lambda_0} > 0$. An elementary computation shows that as long as $\lambda_0 > 0$, this inequality holds. We shall use group theoretic methods developed by Sattinger to study the bifurcation of doubly-periodic solutions to (3.8) near $E = I = 0$, $\lambda = \lambda_0$, and $\omega = \omega_0$.

Because of the covariance of $\mathbf{G}$ with T_g, $T_g \mathbf{G} = \mathbf{G} T_g$, the kernel of $L(\lambda_0)$ consists of a continuous family of critical wave vectors (k_0, ℓ_0) satisfying $k_0^2 + \ell_0^2 = \omega_0^2$:

$$\mathrm{Ker}\, L(\lambda_0) \equiv \eta = \{\Phi(\lambda_0, \omega_0^2) e^{i\langle r\boldsymbol{\omega}_0, x\rangle}\} r \in O(2) \tag{4.7}$$

with $\boldsymbol{\omega}_0 = (\omega_0, 0)$, $\mathbf{x} = (x, y)$, and $\langle \mathbf{x}^1, \mathbf{y}^2 \rangle = x_1 x_2 + y_1 y_2$. This kernel is infinite dimensional so *to reduce the problem to one of finite degeneracy we restrict the solution space to the subclass of doubly-periodic functions.*

§ 5. Doubly-periodic Functions

In Sect. 4, we showed that the kernel $L(\lambda_0)$ had infinite degeneracy. By restricting the solution space to the class of doubly-periodic functions, we can reduce this to finite degeneracy. Let $\boldsymbol{\omega}_1$ and $\boldsymbol{\omega}_2$ be two linearly independent vectors in the plane. A lattice Λ is a set of vectors, $\{\boldsymbol{\omega}\}$ generated by integer combinations of $\boldsymbol{\omega}_1$ and $\boldsymbol{\omega}_2$; i.e., there are integers P_1 and P_2 such that $\boldsymbol{\omega} = P_1 \boldsymbol{\omega}_1 + P_2 \boldsymbol{\omega}_2$. Let $K(\Lambda)$ be the subgroup of translations in the plane which belongs to the lattice:

$$K(\Lambda) = \{T_\omega : \boldsymbol{\omega} \in \Lambda\} .$$

The class of doubly-periodic functions (or more precisely Λ-periodic) are those which are invariant under $K(\Lambda)$, i.e.:

$$(T_\omega \psi)(\mathbf{x}) = \psi(\mathbf{x} + \boldsymbol{\omega}) = \psi(\mathbf{x}); \quad \boldsymbol{\omega} \in \Lambda .$$

This is an obvious generalization of periodicity on the real line. Let $\mathscr{I}(\Lambda) = \{\psi \in \mathscr{I} | \psi \text{ is } \Lambda\text{-periodic}\}$. Clearly because $\mathbf{G}$ is translation invariant, it maps $\mathscr{I}(\Lambda)$ into itself. Let $\mathscr{D}(\Lambda)$ denote the largest subgroup of $O(2)$ leaving Λ invariant. These groups are finite so that the kernel, (4.7), when so restricted has only finite degeneracy:

$$\eta(\Lambda) = \ker L(\lambda_0)|_{\mathscr{I}(\Lambda)} = \{\Phi(\lambda_0, \omega_0^2) e^{i\langle r\boldsymbol{\omega}_0, \mathbf{x}\rangle}\} r \in \mathscr{D}(\Lambda) .$$

$\mathscr{E}(\Lambda)$ is the subgroup of $\mathscr{E}$ leaving $\mathscr{I}(\Lambda)$ invariant and is generated by translations $K(\Lambda)$ and rotation-reflections, $\mathscr{D}(\Lambda)$.

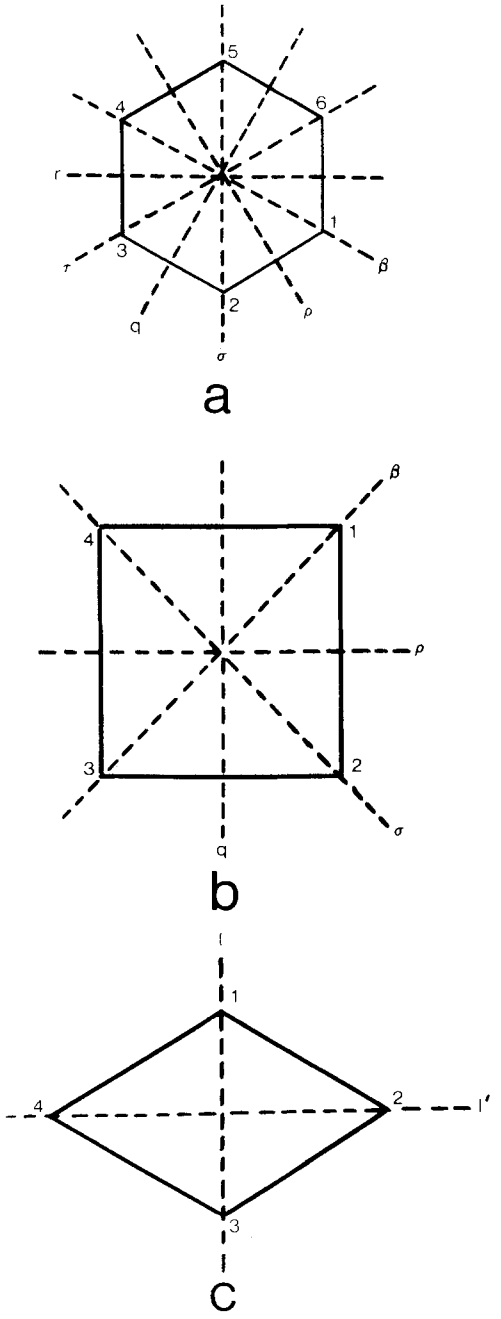

Fig. 6a–c. The basic symmetry groups. **a** Hexagonal. **b** Square. **c** Rhombic

We are interested in lattices generated by $\boldsymbol{\omega}_1$, $\boldsymbol{\omega}_2$ satisfying $|\boldsymbol{\omega}_1|=|\boldsymbol{\omega}_2|=\omega_0$, the critical wave number. The symmetry of the lattice depends solely on the angle, θ, between the two basic vectors. There are three possibilities:

(1) *Hexagonal*, Λ_6. Here the angle between the two basis vectors is 60°, and the holohedry $\mathscr{D}(\Lambda_6)=D_6$, is the symmetry group of the hexagon. It has 12 elements generated by α, a 60° clockwise rotation and β, a reflection about the x-axis (see Table 1a and Fig. 6a).

Table 1[a]. Elements of each of the three symmetry groups

Rotation			Reflection about
a) Hexagonal elements			
$\alpha=(123456)$	60°	$\beta=(53)(26)$	β
$\alpha^2=(135)(246)$	120°	$\alpha\beta=(54)(36)(12)$	ϱ
$\alpha^3(14)(25)(36)$	180°	$\alpha^2\beta=(13)(46)$	σ
$\alpha^4(153)(642)$	−120°	$\alpha^3\beta=(14)(56)(23)$	q
$\alpha^5(165432)$	− 60°	$\alpha^4\beta=(51)(24)$	τ
α^6 identity $\equiv e$	0°	$\alpha^5\beta=(16)(34)(25)$	r
b) Square elements			
$\alpha=(1234)$	90°	$\beta=(24)$	β
$\alpha^2=(13)(24)$	180°	$\alpha\beta=(21)(34)$	ϱ
$\alpha^3=(1432)$	− 90°	$\alpha^2\beta=(13)$	σ
$\alpha^4=$ identity $\equiv e$	0°	$\alpha^3\beta=(14)(23)$	q
c) Rhombic elements			
$\alpha=(13)(24)$	180°	$\beta=(24)$	l
$\alpha^2=$ identity $=e$	0°	$\alpha\beta=(13)$	l'

[a] In listing elements we have made use of cycle notation to show where the vertices go under each symmetry element

The kernel is six-dimensional and consists

$$\psi_1(\mathbf{x})=\Phi_0 e^{i\omega_0 x},\quad \psi_6(\mathbf{x})=T_\alpha\psi_1=\Phi_0 e^{i\omega_0(x/2+y\sqrt{3}/2)},$$
$$\psi_5(\mathbf{x})=T_{\alpha^2}\psi_1=\Phi_0 e^{i\omega_0(-x/2+y\sqrt{3}/2)},$$
$$\psi_4(\mathbf{x})=\bar{\psi}_1(\mathbf{x}),\quad \psi_2(\mathbf{x})=\bar{\psi}_5(\mathbf{x}),$$
$$\psi_3=\bar{\psi}_6(\mathbf{x}),\quad \text{where}\quad \Phi_0\equiv\Phi(\lambda_0,\omega_0^2).$$

(2) *Square*, Λ_4. Here θ is 90°. $\mathscr{D}(\Lambda_4)=D_4$, the symmetry group of the square, and is generated by α, a 90° clockwise rotation, and β, a reflection about the x-axis (see Table 1b and Fig. 6b). There are four basis elements in the kernel:

$$\psi_1(\mathbf{x})=\Phi e^{i\omega_0 x},\quad \psi_4(\mathbf{x})=T_\alpha\psi_1=\Phi_0 e^{i\omega_0 y},$$
$$\psi_3=\bar{\psi}_1,\quad \psi_2=\bar{\psi}_4.$$

(3) *Rhombic*, Λ_2. Here θ is any acute angle other than 90° or 60°. $\mathscr{D}(\Lambda_2)=D_2$, the symmetry group of the rectangle, and is generated by α, a 180° rotation, and β, a reflection along some line, ℓ (see Table 1c and Fig. 6c). The kernel is also four-dimensional and is generated by:

$$\psi_1(\mathbf{x})=\Phi_0 e^{i\omega_0 x},$$
$$\psi_4(x)=T_{\alpha\beta}\psi_1=\Phi_0 e^{i\omega_0(\cos\theta x+\sin\theta y)},$$
$$\psi_3=\bar{\psi}_1,$$
$$\psi_2=\bar{\psi}_4.$$

Because each element of the group can be represented by a permutation, it is clear that for some element $g\in\mathscr{D}(\Lambda)$, $T_g\psi_j=\psi_k$ where ψ_j and ψ_k are the wave functions above. For any vector $\mathbf{a}\in R^2$, we see that $T_{\mathbf{a}}\psi_j=e^{i\langle\boldsymbol{\omega}_j,\mathbf{a}\rangle}\psi_j$, where $\boldsymbol{\omega}_j$ is the wave vector corre-

Table 2. Effects of the representations on the elements of the kernel

a) Hexagonal

$\psi = \sum_{i=1}^{6} z_i \psi_i$

$T_\alpha(z_1, z_2, z_3, z_4, z_5, z_6) = (z_6, z_1, z_2, z_3, z_4, z_5)$

$T_\beta(z_1, z_2, z_3, z_4, z_5, z_6) = (z_1, z_6, z_5, z_4, z_3, z_2)$

$T_{\mathbf{a}}(z_1, \ldots, z_6) = (e^{i\langle \omega_1, \mathbf{a}\rangle} z_1, \ldots, e^{i\langle \omega_6, \mathbf{a}\rangle} z_6)$

b) Square

$\psi = \sum_{i=1}^{4} z_i \psi_i$

$T_\alpha(z_1, z_2, z_3, z_4) = (z_4, z_1, z_2, z_3)$

$T_\beta(z_1, z_2, z_3, z_4) = (z_1, z_4, z_3, z_2)$

$T_{\mathbf{a}}(z_1, z_2, z_3, z_4) = (e^{i\langle \omega_1, \mathbf{a}\rangle} z_1, \ldots, e^{i\langle \omega_4, \mathbf{a}\rangle} z_4)$

c) Rhombic

$T_\alpha(z_1, \ldots, z_4) = (z_3, z_4, z_1, z_2)$

$T_\beta(z_1, z_2, z_3, z_4) = (z_2, z_1, z_4, z_3)$

$T_{\mathbf{a}}(z_1, \ldots, z_4) = (e^{i\langle \omega_1, \mathbf{a}\rangle} z_1, \ldots, e^{i\langle \omega_4, \mathbf{a}\rangle} z_4)$

Table 3. Effect of representations on reduced bifurcation variables

a) Hexagonal

$T_\alpha(x_1, x_2, x_3; \theta_1, \theta_2, \theta_3) = (x_3, x_1, x_2; -\theta_3, \theta_1, \theta_2)$

$T_\beta(x_1, x_2, x_3; \theta_1, \theta_2, \theta_3) = (x_1, x_3, x_2; -\theta_1, -\theta_3, -\theta_2)$

$T_{\mathbf{a}}(x_1, x_2, x_3; \theta_1, \theta_2, \theta_3) = (x_1, x_2, x_3; \theta_1 + \langle \boldsymbol{\omega}_1, \mathbf{a}\rangle, \ldots, \theta_3 + \langle \boldsymbol{\omega}_3, \mathbf{a}\rangle)$

b) Square

$T_\alpha(x_1, x_2; \theta_1, \theta_2) = (x_2, x_1; -\theta_2, \theta_1)$

$T_\beta(x_1, x_2; \theta_2, \theta_2) = (x_1, x_2; -\theta_1, -\theta_2)$

$T_{\mathbf{a}}(x_1, x_2; \theta_1, \theta_2) = (x_1, x_2; \theta_1 + \langle \boldsymbol{\omega}_1, \mathbf{a}\rangle, \theta_2 + \langle \boldsymbol{\omega}_2, \mathbf{a}\rangle)$

c) Rhombic

$T_\alpha(x_1, x_2; \theta_1, \theta_2) = (x_1, x_2; -\theta_1 - \theta_2)$

$T_\beta(x_1, x_2; \theta_1, \theta_2) = (x_2, x_1; \theta_2, \theta_1)$

$T_{\mathbf{a}}(x_1, x_2; \theta_1, \theta_2) = (x_1, x_2; \theta_1 + \langle \boldsymbol{\omega}_1, \mathbf{a}\rangle, \theta_2 + \langle \boldsymbol{\omega}_2, \mathbf{a}\rangle)$

sponding to the j^{th} vertex. For example in the rhombic case, $\boldsymbol{\omega}_1 = (\omega_0, 0)$, $\boldsymbol{\omega}_2 = (\omega_0 \cos\theta, -\omega_0 \sin\theta)$, etc. To see the action of $\mathscr{D}(\Lambda)$ on the kernel, we notice that for any $\psi \in \eta(\Lambda)$, $\psi = \sum_{i=1}^{n} z_i \psi_i$ where $n = 4$ for the square and rhombic cases, and $n = 6$ for hexagonal. Here z_i are complex numbers and since ψ is real we must have $z_j = \bar{z}_k$ if $\psi_j = \bar{\psi}_k$. In Table 2a–c we give the action of the representations on the kernel for each lattice. Since $z_4 = \bar{z}_1$, $z_5 = \bar{z}_2$, $z_6 = \bar{z}_3$ for hexagonal lattices, and $z_3 = \bar{z}_1$, $z_4 = \bar{z}_2$ for rhombic and square, we may write $z_j = x_j e^{i\theta_j}$, $z_{j+3} = x_j e^{-i\theta_j}$, $j = 1, 2, 3$, $x_j \geqq 0$, $\theta_j \in [0, 2\pi)$ for the hexagonal case or $z_j = x_j e^{i\theta_j}$, $z_{j+2} = x_j e^{-i\theta_j}$, $j = 1, 2$, $x_j \geqq 0$, $\theta_j \in [0, 2\pi)$ for the rhombic and square cases. In Table 3a–c we show the group action in these new coordinates. This group structure is readily utilized to determine the new solutions branching from the unstable rest state of the nonlinear problem, $\mathbf{G}(E, I; \lambda) = 0$.

§ 6. Bifurcation and the New Solutions

We are interested in solving the problem:

$$\mathbf{G}(\lambda; \mathbf{u}) = 0, \quad \mathbf{u} \in \mathscr{I}, \tag{6.1}$$

where $\lambda \in R$ and $\mathscr{I}$ is as above. $\mathbf{G}: R \times \mathscr{I} \to \mathscr{I}$, and there is always a solution to (6.1), $\mathbf{u} = 0$, i.e.,

$$\mathbf{G}(\lambda; 0) = 0. \tag{6.2}$$

As long as $D\mathbf{G}(\bar{\lambda}; 0)$ is nonsingular [here $D\mathbf{G}(\bar{\lambda}; 0)$ means the Frechet derivative of $\mathbf{G}$ with respect to $\mathbf{u}$ evaluated at $\mathbf{u} = 0$ and $\lambda = \bar{\lambda}$] the implicit function theorem states there are no other small amplitude solutions to (6.1) near $\lambda = \bar{\lambda}$ and $\mathbf{u} = 0$. On the other hand, if $D\mathbf{G}(\bar{\lambda}; 0)$ has a nonzero kernel, then we no longer obtain uniqueness and the possibility arises that there will be other small amplitudes solutions. The Lyapunov-Schmidt technique allows us to calculate these new solutions. As we can see, this is precisely the situation discussed in § 3: the linearized equation has a nonzero kernel at $\lambda = \lambda_0$.

Assume that at $\lambda = \lambda_0$, $D\mathbf{G}(\lambda_0; 0)$ has an n-dimensional kernel and cokernel. Let $\psi_1, \ldots, \psi_n$ generate the kernel and $\psi_1^*, \ldots, \psi_n^*$ generate the cokernel. Let $E: \mathscr{I} \to \text{range } D\mathbf{G}(\lambda_0; 0)$, so that $(I - E): \mathscr{I} \to \text{coker } D\mathbf{G}(\lambda_0; 0)$. The mapping $(I - E)$ consists of the direct sum of the projections, P_j, $P_j \mathbf{u} = \langle \mathbf{u}, \psi_j^* \rangle \psi_j^*$ for all $\mathbf{u} \in \mathscr{I}$. Let $Q: \mathscr{I} \to \text{kernel } D\mathbf{G}(\lambda_0; 0)$. $(I - Q)$ maps $\mathscr{I}$ into that part of $\mathscr{I}$ not in the kernel of $D\mathbf{G}(\lambda_0; 0)$. Thus $D\mathbf{G}(\lambda_0; 0)$ is one to one as a map from $(I - Q)\mathscr{I}$ onto $E\mathscr{I}$, so there is a map $M = E\mathscr{I} \to (I - Q)\mathscr{I}$ such that $MD\mathbf{G}(\lambda_0; 0) = \text{identity on } (I - Q)\mathscr{I}$. Write the elements of $\mathscr{I}$ as

$$\mathbf{u} = \psi + w, \quad \text{where} \quad \psi = Q\mathbf{u}, \quad w = (I - Q)\mathbf{u}.$$

Rewrite (6.1) as

$$D\mathbf{G}(\lambda_0; 0)\mathbf{u} = -\mathbf{G}(\lambda; \mathbf{u}) + D\mathbf{G}(\lambda_0; 0)\mathbf{u}. \tag{6.3}$$

Apply ME and $(I - E)$ to both sides of (6.3) to obtain:

$$w = ME[-\mathbf{G}(\lambda; w + \psi) + D\mathbf{G}(\lambda_0; 0)(w + \psi)], \tag{6.4a}$$

$$(I - E)\mathbf{G}(\lambda; w + \psi) = 0. \tag{6.4b}$$

(6.4a) can be uniquely solved for $w = w^*(\lambda; \psi)$ for λ near λ_0 and ψ near zero, and this is substituted into (6.4b) obtaining:

$$F(\lambda; \psi) \equiv (I - E)\mathbf{G}(\lambda; \psi + w^*(\lambda; \psi)) = 0. \tag{6.5}$$

For λ fixed, $F: Q\mathscr{I} \to (I - E)\mathscr{I}$. Each of these is an n dimensional space, so $\psi = \sum_{i=1}^{n} z_i \psi_i$ and $F = \sum_{i=1}^{n} F_i \psi_i^*$, thus (6.5) is equivalent to solving the equations:

$$\begin{aligned} &F_1(\lambda; z_1, \ldots, z_n) = 0 \\ &F_2(\lambda; z_1, \ldots, z_n) = 0 \\ &\vdots \\ &F_n(\lambda; z_1, \ldots, z_n) = 0. \end{aligned} \tag{6.6}$$

We call (6.6) the bifurcation equations and solving (6.6) generates a solution to (6.1). Thus the solution set of (6.1) for $|\lambda-\lambda_0|$ and $\|\mathbf{u}\|$ near zero is equivalent to the solution set of (6.6) for $|\lambda-\lambda_0|, |z_i|$ small.

In general, the form of (6.6) is very difficult to compute, but the covariance of (6.1) is preserved for (6.6) and consequently we can simplify calculations immensely. We shall give an example of some of the calculations and then state a theorem due to Sattinger. Each F_j may be written as a sum of linear, quadratic, cubic, etc. terms in the six variables, $z_1, z_2, \ldots, z_6$ (or z_1, z_2, z_3, z_4 in the case of rhombic and square lattices) consider $n=6$, the hexagonal lattice. By the covariance of (6.6)

$$T_{\alpha^5} F = F T_{\alpha^5}. \tag{6.7}$$

That is, $F_2(\lambda; z_1, \ldots, z_6) = F_1(\lambda; z_2, z_3, z_4, z_5, z_6, z_1)$, etc. Thus if we find F_1, we can obtain $F_2, F_3, \ldots, F_6$ by appropriate permutations of the variables. Since (6.1) is real, $F_1(\lambda; z_1, \ldots, z_6) = F_1(\lambda; \bar{z}_1, \ldots, \bar{z}_6)$. Finally

$$e^{i\langle \omega_1, \mathbf{a}\rangle} F_1(\lambda; z_1, \ldots, z_6) = F_1(\lambda; e^{i\langle \omega_1 \mathbf{a}\rangle} z_1, \ldots, e^{i\langle \omega_6, \mathbf{a}\rangle} z_6). \tag{6.8}$$

Let us look at the separate linear, quadratic, etc. terms of F_1. Consider as an example the cubic terms, $z_i z_j z_k$. From (6.8),

$$e^{i\langle \omega_1, \mathbf{a}\rangle} \sum_{1 \leqq i \leqq j \leqq k \leqq 6} k_{ijk} z_i z_j z_k = \sum_{1 \leqq i \leqq j \leqq k \leqq 6} e^{i\langle \omega_i + \omega_j + \omega_k, \mathbf{a}\rangle} z_i z_j z_k.$$

Since this is true for all $\mathbf{a}$ we must have

$$\boldsymbol{\omega}_i + \boldsymbol{\omega}_j + \boldsymbol{\omega}_k = \boldsymbol{\omega}_1$$

or $\boldsymbol{\omega}_i = \boldsymbol{\omega}_1$ and $\boldsymbol{\omega}_k = -\boldsymbol{\omega}_j$. Thus there are terms of the form:

$$z_1 z_1 z_4, z_1 z_2 z_5, z_1 z_3 z_6.$$

Since $T_\beta F = F T_\beta$, $z_1 z_2 z_5$ and $z_1 z_3 z_6$ must have the same coefficient. Finally the complex conjugacy requirement implies that the coefficients of these terms are real. Hence the cubic terms are

$$b z_1 (z_3 z_6 + z_2 z_5) + a z_1 z_1 z_4; \; a, b \in R.$$

The coefficients a and b depend on the lattice, λ, and the physical parameters of the system. We can similarly compute the linear, quadratic, and higher order terms of F_1. These are still complex valued functions and they have a certain degeneracy which is avoided by using the variables, $(x_1, x_2, x_3; \theta_1, \theta_2, \theta_3)$ or $(x_1, x_2; \theta_1, \theta_2)$ for square and rhombic lattices. To this end we have the following theorem.

Theorem 6.1 (Sattinger, 1978a). *The reduced bifurcation equations for the bifurcation of Λ-periodic disturbances of a Euclidean covariant system,* (6.1) *have the forms below:*

(1) *Λ = rectangular or square lattice*

$$x_1(\lambda + a x_1^2 + b x_2^2) = O(\lambda x_i x_j, x_i x_j x_k x_l)$$
$$x_2(\lambda + a x_2^2 + b x_1^2) = O(\lambda x_i x_j, x_i x_j x_k x_l).$$

(2) *Λ = hexagonal lattice with nonvanishing quadratic terms*

$$\lambda x_1 - c e^{i\gamma} x_2 x_3 = O(\lambda x_i x_j, x_i x_j x_k)$$
$$\lambda x_2 - c e^{i\gamma} x_2 x_3 = O(\lambda x_i x_j, x_i x_j x_k)$$
$$\lambda x_3 - c e^{i\gamma} x_1 x_2 = O(\lambda x_i x_j, x_i x_j x_k).$$

(3) *Λ = hexagonal lattice with vanishing quadratic terms*

$$x_1(\lambda + b(x_2^2 + x_3^2) + a x_1^2) = O(\lambda x_i x_j, x_i x_j x_k x_l)$$
$$x_2(\lambda + b(x_1^2 + x_3^2) + a x_2^2) = O(\lambda x_i x_j, x_i x_j x_k x_l)$$
$$x_3(\lambda + b(x_1^2 + x_2^2) + a x_3^2) = O(\lambda x_i x_j, x_i x_j x_k x_l).$$

Remarks. When the thresholds are zero and the nonlinearities of our neural net are symmetric, the second case does not occur since $c=0$. The parameters a and b are not the same numerically and depend on the lattice type as well as the actual physical parameters of the system. We shall not consider case (2) since in all previous work we have assumed no quadratic terms exist. We are interested in small amplitude solutions to (1) and (3), so we put $\lambda = \varepsilon^2 \nu$ and $x_i = \varepsilon y_i$, where $\varepsilon \to 0$ is a small number. With this scaling we obtain for example:

$$\varepsilon^3 y_1(\nu + a y_1^2 + b y_2^2) = 0(\varepsilon^4).$$

Dividing by ε^3 and letting $\varepsilon \to 0$ leads to the bifurcation equations for small amplitude solutions:

(1) $y_1(\nu + a y_1^2 + b y_2^2) = 0$
$y_2(\nu + a y_2^2 + b y_1^2) = 0.$

(3) $y_1(\nu + b(y_2^2 + y_3^2) + a y_1^2) = 0$
$y_2(\nu + b(y_1^2 + y_3^2) + a y_2^2) = 0$
$y_3(\nu + b(y_1^2 + y_2^2) + a y_3^2) = 0.$

Consequently to lowest order the solution to (6.1) or, for that matter, (3.7), is:

$$\begin{bmatrix} E(x,y) \\ I(x,y) \end{bmatrix} = \varepsilon \Phi(\lambda_0, \omega_0^2) \operatorname{Re}\left[y_1 e^{i\theta_1} e^{i\langle \omega_1, \mathbf{x}\rangle} + y_2 e^{i\theta_2} e^{i\langle \omega_2, \mathbf{x}\rangle} \right] + O(\varepsilon^2),$$
$$\lambda = \varepsilon^2 \nu + O(\varepsilon^3), \; \mathbf{x} = (x, y) \tag{6.10}$$

Table 4. Solutions to bifurcation equations for rhombic or square and hexagonal lattices

Case	Solution	Eigenvalues
(1)	$y_2=0, y_1=\sqrt{\frac{-v}{a}}$	$-2v, \frac{-v(b-a)}{a}$
	$y_1=y_2=\sqrt{\frac{-v}{a+b}}$	$-2v, -2v\frac{(a-b)}{(a+b)}$
(3)	$y_2=y_3=0, y_1=\pm\sqrt{\frac{-v}{a}}$	$-2v, \frac{-v}{b}(a-b), \frac{-v}{b}(a-b)$
	$y_3=0, y_1=y_2=\sqrt{\frac{-v}{a+b}}$	$v\frac{b-a}{a+b}, -2v, -2v\frac{(b-a)}{(a+b)}$
	$y_1=y_2=y_3=\sqrt{\frac{-v}{2a+b}}$	$-2v, \frac{-2v(b-a)}{2a+b}, \frac{-2v(b-a)}{2a+b}$

for rhombic and square lattices and

$$\begin{bmatrix}E(x,y)\\I(x,y)\end{bmatrix}=\varepsilon\Phi(\lambda_0,\omega_0^2)R_e[y_1e^{i\theta_1}e^{i\langle\omega_1,\mathbf{x}\rangle}+y_2e^{i\theta_2}e^{i\langle\omega_2,\mathbf{x}\rangle}+y_3e^{i\theta_3}e^{i\langle\omega_3\mathbf{x}\rangle}]+O(\varepsilon^2),\quad(6.1)$$
$$\lambda=\varepsilon^2v+O(\varepsilon^3),\qquad\mathbf{x}=(x,y)$$

for hexagonal lattices.

For $v>0$, we have supercritical bifurcation, while for $v<0$ subcritical, and y_i are solutions to (1) or (3). In both cases there are two or three arbitrary phase factors due to the translation invariance of (6.1). In Table 4 we give the solutions to (6.9), (1), (3) as well as the eigenvalues of the Jacobian evaluated at the solutions, y_i. By Theorem 7.2 in Sattinger, the solutions (6.10) and (6.11) are stable or unstable if the eigenvalues of the Jacobian have negative real parts or not. We note that Table 4 does not give a complete list of solutions, for example $y_1=0$, $y_2=\sqrt{-\frac{v}{a}}$ is also a solution, but it is qualitatively the same as $y_2=0$, $y_1=\sqrt{-\frac{v}{a}}$, with the same stability. In the next section, we explore the stability of the various solutions and the concomitant form constants arising from each solution. We shall show how the physical parameters of the neural net act to "select" the stable spatial patterns of activity.

§ 7. Stability and Selection of Forms

Before discussing stability and the dependence of a and b on the lattice, we wish to show the meaning of the various solutions in terms of the form constants of Klüver. From (6.10) and (6.11) we know the electrical pattern of activity to lowest order. In the following figures and paragraphs, we shall examine these solutions and their symmetry properties.

a) Rhombic and square lattices

Case (i) $y_1=0,\quad y_2\neq0;$ or $y_2=0,\quad y_1\neq0.$

In the case of a square lattice we have

$$\begin{pmatrix}E(x)y)\\I(x,y)\end{pmatrix}=\varepsilon\Phi(\lambda_0,\omega_0^2)\sqrt{\frac{-v}{a}}\cos[\theta_1+\omega_0x];$$
$$y_2=0,\qquad(7.1a)$$
$$\begin{pmatrix}E(x,y)\\I(x,y)\end{pmatrix}=\varepsilon\Phi(\lambda_0,\omega_0^2)\sqrt{\frac{-v}{a}}\cos[\theta_2+\omega_0y];$$
$$y_1=0;\qquad(7.1b)$$

While for the rhombic we have

$$\begin{pmatrix}E(x,y)\\I(x,y)\end{pmatrix}=\varepsilon\Phi(\lambda_0,\omega_0^2)\sqrt{\frac{-v}{a}}\cos[\theta_2+c\omega_0x+s\omega_0y],$$
$$y_1=0;\quad c=\cos\theta,\quad s=\sin\theta.\qquad(7.1c)$$

All three cases are shown in Fig. 7 where we have plotted only $E(x,y)$. These are all constant along some line and thus lead to spiral, tunnel, of funnel form constants. We call these patterns "rolls" after the term used for such forms in fluid mechanics, and see that they give rise to the "global" type of form constant.

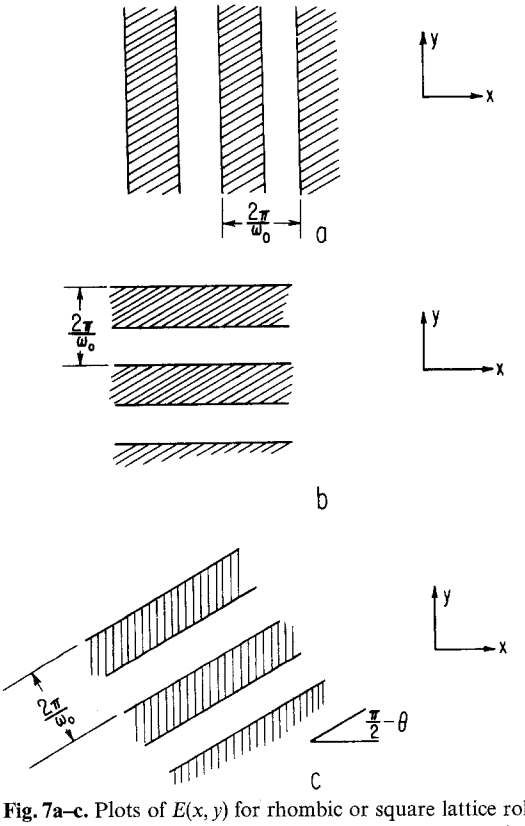

Fig. 7a–c. Plots of $E(x,y)$ for rhombic or square lattice roll patterns (shaded regions are positive). **a** Pattern leading to tunnel constant. **b** Pattern leading to funnel constant. **c** Pattern leading to spiral constant (occurs in rhombic lattice only)

Case (ii) $y_1 = y_2 = \sqrt{\frac{-v}{a+b}}$.

For a square lattice we have

$$\begin{pmatrix} E(x,y) \\ I(x,y) \end{pmatrix} = \varepsilon \Phi(\lambda_0, \omega_0^2) \sqrt{\frac{-v}{a+b}} \{\cos[\theta_1 + \omega_0 x] + \cos[\theta_2 + \omega_0 y]\} \quad (7.2a)$$

while for a rhombic lattice we have

$$\begin{pmatrix} E(x,y) \\ I(x,y) \end{pmatrix} = \varepsilon \sqrt{\frac{-v}{a+b}} \Phi(\lambda_0, \omega_0^2) \cdot \{\cos[\theta_1 + \omega_0 x] + \cos[\theta_2 + \omega_0 (cx + sy)]\}. \quad (7.2b)$$

For various values of θ, we have graphed these functions for cases (a) and (b), in Fig. 8. In particular we have plotted a detailed picture of contours of $E \equiv$ constant, for various θ_1, θ_2 for (7.2a).

Clearly these patterns all have true double periodicity and give rise to cobweb and lattice form constants. Depending on the stability of the two cases, we should expect to observe either local tesselation patterns (repeating mosaics, cobwebs) or global spirals, tunnels, and funnels.

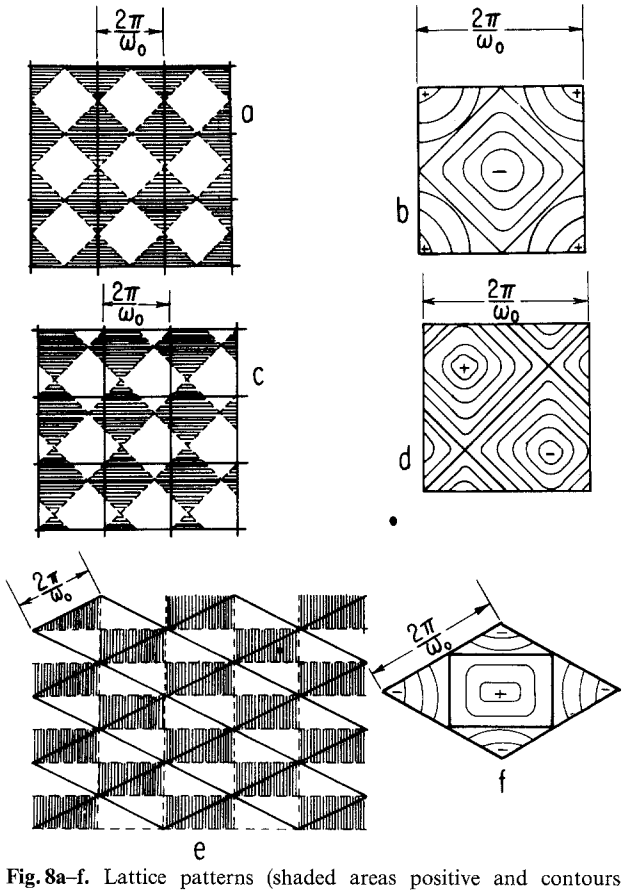

Fig. 8a–f. Lattice patterns (shaded areas positive and contours represent $E(x,y) =$ constant). **a** Square pattern, $\theta_1 = \theta_2 = 0$. **b** Contours of (a) for single square. **c** Square pattern, $\theta_1 = -90, \theta_2 = 90$. **d** Contours of (c) for single square. **e** Rhombic pattern $\theta_1 = \theta_2 = 180°$. **f** Contours of (e) for single rhombus

b) Hexagonal lattices

Case (i) $y_2 = 0, \quad y_3 = 0, \quad y_1 \neq 0$.

We obtain:

$$\begin{pmatrix} E(x,y) \\ I(x,y) \end{pmatrix} = \varepsilon \sqrt{\frac{-v}{b}} \Phi(\lambda_0, \omega_0^2) \cos[\theta_1 + \omega_0 x] \quad (a)$$

or if $y_1 = y_3 = 0; \; y_2 \neq 0$

$$\begin{pmatrix} E(x,y) \\ I(x,y) \end{pmatrix} = \varepsilon \sqrt{\frac{-v}{b}} \Phi(\lambda_0, \omega_0^2) \cos\left[\theta_2 + \frac{\omega_0}{2} x + \frac{\omega_0 \sqrt{3} y}{2}\right] \quad (b)$$

and a similar expression for $y_1 = y_2 = 0; \; y_3 \neq 0$.

Case (ii) $y_1 = y_2 = \sqrt{\frac{-v}{a+b}}, \quad y_3 = 0$.

This and the remaining always have a pair of eigenvalues with opposite signs, $v\frac{a-b}{a+b}$ and $-2v\left(\frac{a-b}{b+a}\right)$, thus they are always unstable and shall not be considered.

Case (iii) $y_1 \neq 0, \quad y_2 \neq 0, \quad y_3 \neq 0$

$$\begin{bmatrix} E(x,y) \\ I(x,y) \end{bmatrix} = \varepsilon \sqrt{\frac{-v}{2b+a}} \Phi(\lambda_0, \omega_0^2) \cdot \left\{\cos[\omega_0 x + \theta_1] + \cos\left[\omega_0\left(\frac{x}{2} - \frac{\sqrt{3} y}{2}\right) + \theta_2\right] + \cos\left[\omega_0\left(\frac{-x}{2} - \frac{\sqrt{3} y}{2}\right) + \theta_3\right]\right\}.$$

For case (i) we illustrate two possibilities in Fig. 9a and b, both of which lead to roll patterns and consequent targets and spirals. In no case do the form constants of the type in Fig. 2d arise. The most interesting situation occurs with case (iii). In Fig. 10 we plot various possibilities for θ_1, θ_2, θ_3 taking of different values. When $\theta_1 = \theta_2 = \theta_3 = 0$, the local pattern is completely hexagonally symmetric as can be seen in Fig. 10a. There are infinitely many such patterns parameterized by θ_1, θ_2, and θ_3, but globally the entire mosaic will always be hexagonal.

Thus far we have considered the various possible solutions to (3.7) but have not yet determined which patterns will actually be "observed". As expected, this depends on certain physiological and physical parameters as well as the initial disturbance. We shall discover that there are certain rules of selection of the form constants but that there is considerable overlap. *Our main assumption is that only stable patterns are observ-*

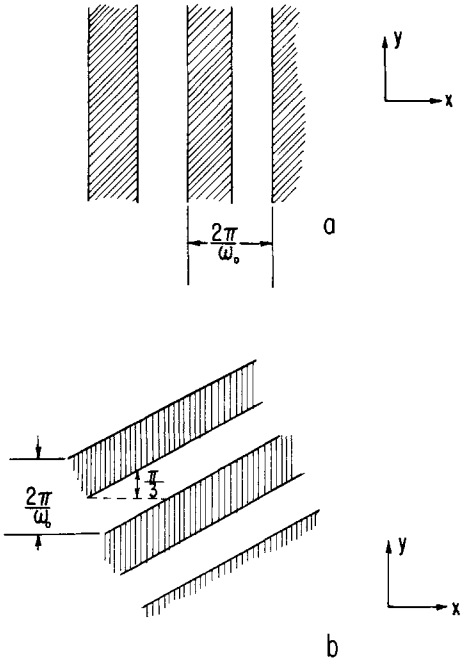

Fig. 9a and b. Roll patterns for hexagonal lattice (shaded areas positive). **a** Pattern leading to funnel. **b** Pattern leading to spiral

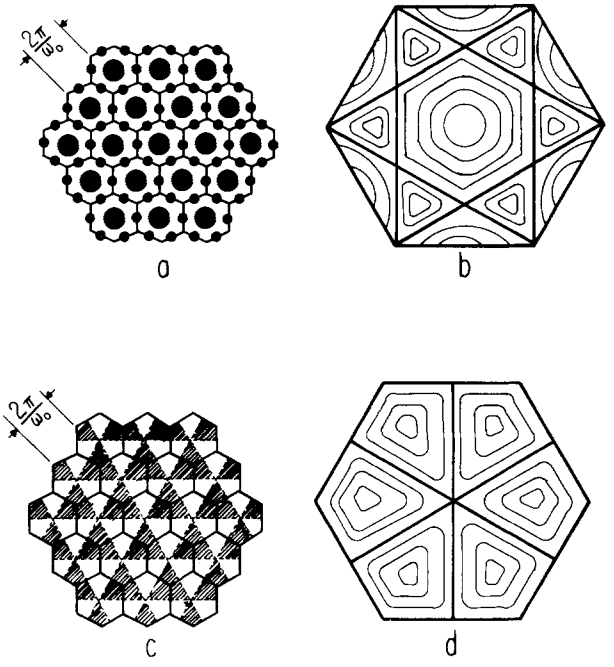

Fig. 10a–d. Hexagonal lattice patterns [shaded areas positive and contours represent $E(x,y)=\text{const}$]. Hexagonal pattern, $\theta_1=\theta_2=\theta_3=0$. **b** Contours if (a) for single hexagon. **c** Hexagonal pattern, $\theta_1=90$, $\theta_2=\theta_3=0$. **d** Contours of (c) for single hexagon

ed. This is reasonable and has been the basis of various models of pattern formation in biological systems. To this end we have the following lemma based on Table 4.

Lemma 7.1 (Sattinger, 1978a). *Assume the bifurcation equations are generated by* (6.09, (1)). *Then the following conditions are necessary for the stability of rolls or squares/rectangles:*

$$\begin{aligned} &\textit{Stable rolls: } b<a<0. \\ &\textit{Stable squares/rectangles: } a+b<0,\ a-b<0. \end{aligned} \tag{7.5a}$$

For hexagonal lattices where the bifurcation equations are generated ny (6.04, (2)) *the necessary conditions for stability are*

$$\begin{aligned} &\textit{Stable rolls: } b<a<0. \\ &\textit{Stable hexagons: } a<b,\ 2b+a<0. \end{aligned} \tag{7.4b}$$

Unfortunately these criteria are still inadequate since a and b both depend on the lattice. To obtain any results on pattern selection we must determine the dependence of a and b on the lattice. Sattinger has proved the following result:

Theorem 7.2 (Sattinger, 1978b). *There exists a function $q(\theta)$, called the lattice function, such that:*

(1) $q(\theta)=A_0+A_2\cos 2\theta+A_4\cos 4\theta$,

(2) $a=3q(0)$, $b=6q(\theta)$,

where θ is the angle between the basis vectors of the lattice and the coefficients A_0, A_2, depend only on the basis physical parameters of the problem.

In many cases $q(\theta)$ is constant while in others it may be written as $q(\theta)=A_0+A_2\cos 2\theta$. In this particular situation, the stability criteria are readily illustrated.

Theorem 7.3 (Sattinger, 1978b). *Suppose $q(\theta)$ may be written as $q(\theta)=A\cos 2\theta+B$. Then the following pattern selection diagram holds:*

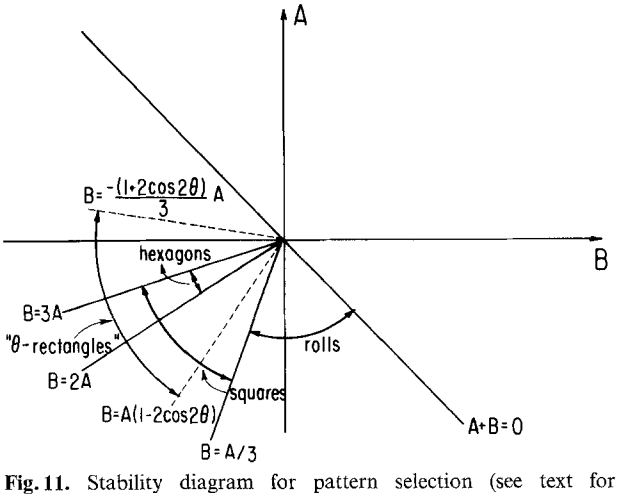

Fig. 11. Stability diagram for pattern selection (see text for explanation)

Thus between $B=\frac{A}{3}$ and $B=2A$ stable hexagons, squares and sometimes "θ-rectangles" (rectangular lattices with basic angle, θ) can coexist. Between $B=2A$ and $B=3A$ only stable squares and certain "θ-rectangles" can coexist. Between $B=3A$ and $A+B=0$, rolls and thus "global" form constants appear, while between $B=-\left(\frac{1+2\cos 2\theta}{3}\right)A$ and $B=\frac{A}{3}$, "θ-rectangles" alone exist. We can imagine that in regions of coexistence, external stimuli and initial conditions will play an important role in pattern selection. As certain physiological parameters change, e.g., excitability or thresholds, we can expect slow transitions between a variety of "cellular" patterns such as cobwebs and honeycombs to spirals and targets. Although the forms seen are "relatively" stationary (i.e., they change at a much slower rate than the time constant of the individual neurons, 10 ms they do indeed slowly change, forming a kaleidoscope of shapes and mosaics as various internal parameters are slowly altered.

§ 8. Discussion

We have shown that a neuronal net comprising a spatially homogeneous two-dimensional sheet of both excitatory and inhibitory neurons, in which the interconnections are all radially isotropic, and in which lateral interactions of negative feedback type, rather than recurrent positive interactions dominate, can spontaneously generate a variety of doubly-periodic spatial patterns of neural activity. If we suppose that these patterns correspond to perceived retinal objects, then the doubly-periodic patterns will be identically the four "form constants" of perceived visual hallucinations. We have demonstrated that physiological parameters play a major role in the selection of form constants, but that such parameters are not in themselves a sufficient explanation for the appearance of unique form constants. The selection mechanism is in fact *dynamical*, and we have therefore utilized bifurcation theory and groups representation theory extensively, to show how stability properties underlie the selection of form constants.

The assumed radial isotropy of intercortical connectivity was exploited to discern the dominant nonlinear effects in the neighborhood of an instability of the net activity. In reality cortical connectivity is far from isotropic (Cowan, 1977) and our analysis must be thought of as heuristic. Rather than $\mathbf{G}(E, I)$ commuting with the entire rotation-reflection group, it is covariant only with a finite subgroup. In such a case $\mathrm{Ker}\, L(\lambda_0)$ is finite-dimensional, and anatomical and physiological constraints determine the symmetry, rather than the ad hoc assumptions of doubly periodic solutions. It is even possible that the only element in $O(2)$ which commutes with $\mathbf{G}$ is the identity. In such a case it can be shown that only small amplitude rolls obtain, and there are no cellular form constants.

We consider this approach to have provided a reasonable description and explanation for the onset of simple visual hallucinations. Clearly as the stages of hallucinatory activity become increasingly advanced, more cortical machinery will be involved, and more complex context-dependent forms may be expected to appear. Our results indicate that it is probably unnecessary to invoke any such complicated processing to account for the ubiquity of simple mosaics and geometric patterns.

Appendix

A. Covariance of G

We must show that $\mathbf{G}$ is covariant with respect to the representation, T_g, defined by

$$T_g u(x, y) = u(g^{-1}(x, y)). \tag{A1}$$

Without loss in generality we suppose $u: R^2 \to R$, that is, we restrict the argument to a single neuronal population. We may write $G(u)(x, y)$ as

$$-u(x, y) + S\left(\alpha \int_{-\infty}^{\infty} dx' \int_{-\infty}^{\infty} dy' w((x-x')^2 + (y-y')^2) u(x', y')\right).$$

Clearly T_g commutes with the identity, thus we examine

$$S(\alpha w(x, y) ** u(x, y)) \equiv S(u).$$

Let $(\bar{x}, \bar{y}) = g^{-1}(x, y)$; $(\bar{x}', \bar{y}') = g^{-1}(x', y')$.

$$T_g S = S\left(\sigma \int_{-\infty}^{\infty} dr' \int_{-\infty}^{\infty} dy' w((x-x')^2 + (y-y')^2) u(x', y')\right). \tag{A2}$$

On the other hand

$$S T_g u = S\left(\alpha \int_{-\infty}^{\infty} dx' \int_{-\infty}^{\infty} dy' w((x-x')^2 + (y-y')^2) u(\bar{x}', \bar{y}')\right).$$

To evaluate this we make the substitution $dx'dy' \to d\bar{x}'d\bar{y}'$. This multiplies by ± 1 so the change of variables has no effect on the integration. The convolution becomes

$$S T_g u = S\left(\alpha \int_{-\infty}^{\infty} d\bar{x}' \int_{-\infty}^{\infty} d\bar{y}' w((\bar{x}-\bar{x}')^2 + (\bar{y}-\bar{y}')^2) u(\bar{x}', \bar{y}')\right) \tag{A3}$$

which is identical to (A2). We remark that if w depended on x and y in an anisotropic fashion, e.g., $w(x,y)=w(x^2/\sigma_1^2+y^2/\sigma_2^2)$; $\sigma_1+\sigma_2$, then we could not obtain (A3). Thus for covariance isotropy is very important.

B. Some Remarks on the Banach Spaces Involved in (3.8)

We may write $G=I+k$, where I is the identity and k is the remaining nonlinear, spatial operator. Let $\mathcal{I}(\Lambda)$ be the Banach space of Λ-periodic functions on the plane, where Λ is fixed. Then k, restricted to $\mathcal{I}(\Lambda)$, is compact so that G is a Fredholm operator, a perturbation of the identity.

We define an inner product structure:

$$\langle u(x,y), v(x,y)\rangle = \int_C u(x,y)\cdot v(x,y)\,dx\,dy\,. \tag{B1}$$

Here C is a unit "cell" in the lattice and $u\cdot v$ is the Euclidean vector product. The linearized operator, $DG(\lambda_0,0)$ is a Fredholm map with *zero* index and a finite dimensional kernel. The projection onto the kernel and cokernel can easily be defined in terms of the inner product, (B1):

$$P_n u=\langle \psi_n(x,y), u(x,y)\rangle \psi_n(x,y)\,, \tag{B2}$$

where $\psi_n(x,y)$ is a normalized basis element of the kernel, $\eta(\Lambda)$. Similar definitions of projections E, Q, etc., hold and the analysis of Sect. 6 can be applied to (3.8) where so restricted.

References

Adey, W.R., Bell, F.R., Dennis, B.J.: Effects of LSD-25, psilocybin, and psilocin on temporal lobe EEG patterns and learned behavior in the cat. Neurology **12**, 591–602 (1962)

Aghajanian, G.K., Foot, W.F., Sheard, M.H.: Action of psychotogenic drugs on single midbarin raphe neurons. J. Pharmacol. Exp. Ther. **171**, 178–187 (1970)

Brawley, P., Duffield, J.C.: The pharmacology of the hallucinogens. Pharm. Rev. **24**, 31–66 (1972)

Cowan, J.D.: Some remarks on channel bandwidths for visual contrast detection. Neurosci. Res. Program Bull. **15**, 492–517 (1977)

Cowan, J.D.: The possible role of development in the specification of the afferent geometry of the primate visual cortex (to appear) (1978)

Demetrescu, M.: Ascending inhibitory and facilitatory influences controlling primary thalamo-cortical responsiveness. Brain Res. **6**, 36–47 (1967)

Dybowski, M.: Conditions for the appearance of hypnagogic visions. Kwart. Psychol. **11**, 68–94 (1939)

Ermentrout, G.B., Cowan, J.D.: Temporal oscillations in neural nets. J. Math. Biol. (1978)

Fischer, B.: Overlap of receptive field centers and representation of the visual field in the cat's optic tract. Vision Res. **13**, 2113–2120 (1973)

Fuxe, K.: Evidence for the existence of monoamine neurons in the central nervous system. IV. The distribution of monamine terminals in the CNS. Acta Physiol. Scand. **64**, Suppl. 247, 41–85 (1965)

Horowitz, M.J., Adams, J.E., Rutkin, B.B.: Evoked hallucinations in epilepsy. Psychiatr. Speculator **11**, 4 (1967)

Klüver, H.: Mescal and the mechanisms of hallucination. Chicago: University of Chicago Press 1967

Krill, A.E., Alpert, H.J., Ostfield, A.M.: Effects of a hallucinogenic agent in totally blind subjects. Arch. Ophthalmol. **69**, 180–185 (1963)

Lance, J.W.: Simple formed hallucinations confined to an area of specific visual defect. Brain **99**, 729–734 (1976)

Penfield, W., Perot, P.: The brain's record or auditory and visual experience, a final summary and discussion. Brain **86**, 595–696 (1963)

Pieri, L., Keller, H.H., Burkard, W., DaPrada, M.: Effects of lisurside and LSD on cerebral monoamine systems and hallucinosis. Nature **272**, 278–280 (1978)

Richards, W.: The fortifiction illusions of migraines. Scient. Amer. **224**, 88–96 (1971)

Sattinger, D.H.: Group representation theory, bifurcation theory, and pattern formation. J. Functional Analysis **28**, 58–101 (1978a)

Sattinger, D.H.: Selection mechanisms for pattern formation. Arch. Rat. Mech. Analys. **66**, 31–42 (1978b)

Schwartz, E.: Spatial mapping in the primate sensory projection: Analytic structure and relevance to perception. Biol. Cybernetics **25**, 181–194 (1977)

Schwindt, P.C.: Membrane potential trajectories underlying motoneuron rhythmic firing at high rates. J. Neurophysiol. **36**, 434–449 (1973)

Siegel, R.K.: Hallucinations. Sci. Am. **237**, 132–140 (1977)

Siegel, R.K.: Cocaine hallucinations. Am. J. Psychiatry **135**, 309–314 (1978)

Winters, W.D., Wallach, M.B.: During induced states of CNS excitation: a theory of hallucinosis. In: Psychotomimetric drugs, pp. 193–214. Efron, D.H. (ed.) New York: Raven Press 1970

Received: May 2, 1979

Prof. J. D. Cowan
Department of Biophysics and
Theoretical Biology
Cummings Life Center
920 East 58th Street
Chicago, IL 60637, USA